[Article] www.whxb.pku.edu.cn

Ni(111)表面上 N 原子对 C 原子电子结构的影响

刘以良[1] 杨缤维[1,2] 蒋 刚[1,*]

([1]四川大学原子与分子物理研究所, 成都 610065; [2]中国工程物理研究院, 四川 绵阳 621900)

摘要: N 是金刚石中的主要杂质之一, 为了研究金刚石生长过程中杂质 N 对 C 电子结构转化的影响, 用密度泛函理论研究了 Ni(111)表面上 C 与 N 共吸附的三个不等价模型, 同时建立了三个 C 吸附模型作为比较. 计算结果表明, N 原子的出现使得吸附体系相对不稳定, 吸附原子之间的相互作用不能忽略; 通过比较相互作用能可以看出, 相同的吸附位下 C–C 相互作用比 C–N 相互作用强. 通过比较不同模型中 C 原子分波态密度可以看出, N–C 相互作用一定程度上增加了 Ni 的催化活性, 但是与 C–C 自身的相互作用比较起来效果并不明显. 吸附几何结构和分波态密度还表明, 当吸附的原子过于紧密以致占有同一个 Ni(111)-(1×1)晶胞表面时, 就会形成 CN 化合物或者类石墨杂质.

关键词: 共吸附; 吸附能; 相互作用能; 分波态密度

中图分类号: O647; O641

Electronic Effects of Atomic Nitrogen on Carbon on the Ni(111) Surface

LIU Yi-Liang[1] YANG Bin-Wei[1,2] JIANG Gang[1,*]

([1]*Institute of Atomic and Molecular Physics, Sichuan University, Chengdu 610065, P. R. China*;
[2]*Chinese Academy of Engineering Physics, Mianyang 621900, Sichuan Province, P. R. China*)

Abstract: Nitrogen is a common impurity found in diamonds. We used three nonequivalent models to study carbon and nitrogen coadsorption on Ni(111) surface. Density functional theory (DFT) calculations were performed to study the influence of nitrogen upon the transformation of carbon′s electronic structure during diamond synthesis. Three carbon adsorption models were constructed for comparison. Results indicated that nitrogen atoms destabilize the adsorption system and that the interaction between adatoms could not be ignored. According to the calculated interaction energies, the C–C interaction was stronger than the C–N interaction. Differences in the partial density of states (PDOSs) among the models suggested that the N–C interaction also improved catalysis to some extent, but this effect was not evident in comparison to the C–C interaction. The obtained atomic geometry and PDOS also indicated formation of CN compounds or graphite-like impurities if the adatom distance was too short, because they would occupy the same Ni(111)-(1×1) unit cell.

Key Words: Coadsorption; Adsorption energy; Interaction energy; Partial density of states

It is well known that the impurities influence significantly on the physical properties of diamond, including the mechanical, thermal, optical, and electronic properties[1–5]. Several impurities exist in the inclusion, and nitrogen is the most dominant atomic impurity found in diamond[4,6]. Physical properties of diamond are influenced significantly by the concentration and forms of nitrogen[7–11], and accordingly, diamonds are classified into types Ia, Ib, IIa, and IIb in terms of the concentration and forms of nitrogen and boron. Numbers of methods are being improved to synthesize diamond and films[12,13]. Experimental results indicated that the nucleation of diamond was inhibited by nitrogen atoms[14]. It is an interesting topic to know how the nitrogen atoms inhibit the growth of diamond on the catalyst surface, especially with microscopic electronic structure method, and for

Received: October 8, 2008; Revised: December 10, 2008; Published on Web: December 30, 2008.

*Corresponding author. Email: gjiang@scu.edu.cn; Tel: +8628-85408810

which the *ab initio* level calculations provide a reliable and accurate way.

In our previous work[15], a model of carbon atom adsorption on the Ni(111) surface was used to interpret the catalytic action of nickel in diamond growth. And the computational results showed that the number of orbitals at the Fermi level was an important criterion for the catalyst effect. Therefore, in order to study the influence of atomic nitrogen on the electronic structure of carbon in diamond synthesis, some models of carbon and nitrogen coadsorption on the Ni(111) surface were built and investigated. However, the computational burden imposed by various ratios of carbon to nitrogen and different adsorption sites made it almost unfeasible. To address this challenge, some simplified adsorption models were built.

In the present work, three nonequivalent models of atomic carbon and nitrogen coadsorbed on the Ni(111)-(2 × 2) surface at a coverage of 0.25 monolayer (ML) were built. Their corresponding C adsorption models were also built for comparison. The atomic geometry, energy, and electronic structure were calculated. The different adsorption energies, interaction energies and density of states (DOS) of the adsorbates are analyzed to recover the electronic effects of atomic nitrogen on carbon.

1 Theoretical methods and models

The Cambridge sequential total energy package (CASTEP) in Material Studio 4.0 (MS) program was used in our work[16], which is a DFT code with plane-wave basis set. All of the calculations are performed using the ultrasoft pseudopotentials[17] and generalized gradient approximation (GGA)[18-20] with a specific functional PBE proposed by Perdew, Burke and Ernzerhof in 1996[20]. The widely used slab model was employed to build our surface models. The essential aim of this article is the comparison of the adsorption energies and the number of orbitals at their Fermi levels among the different models, and Ref. [15] indicated that three-layer substrate was enough to show the catalysis of Ni, moreover, our computational adsortption energies of C atom are 7.299 and 7.350 eV at fcc and hcp hollow sites, respectively, which agree with the very scare experimental data of 7.01 eV[21]. Therefore, to reduce the computational burden, the metal substrate was represented by a three-layer slab for Ni by a 1.2 nm thick vacuum region. The bulk Ni lattice parameters used in all models were first obtained using a plane-wave energy cutoff of 350.0 eV and the Monkhorst-Pack *k*-point grid of 8×8×8 within the Brillouin zone, and the calculated value of 0.354 nm agreed well with the experimental value of 0.352 nm[22,23]. In order to show more realistic adsorption energies and (P)DOS, the experimental lattice parameter 0.352 nm was used to build the surface models.

In view of the translational invariance of the Ni(111)-(2×2) supercell and the calculated slight adsorption energy difference

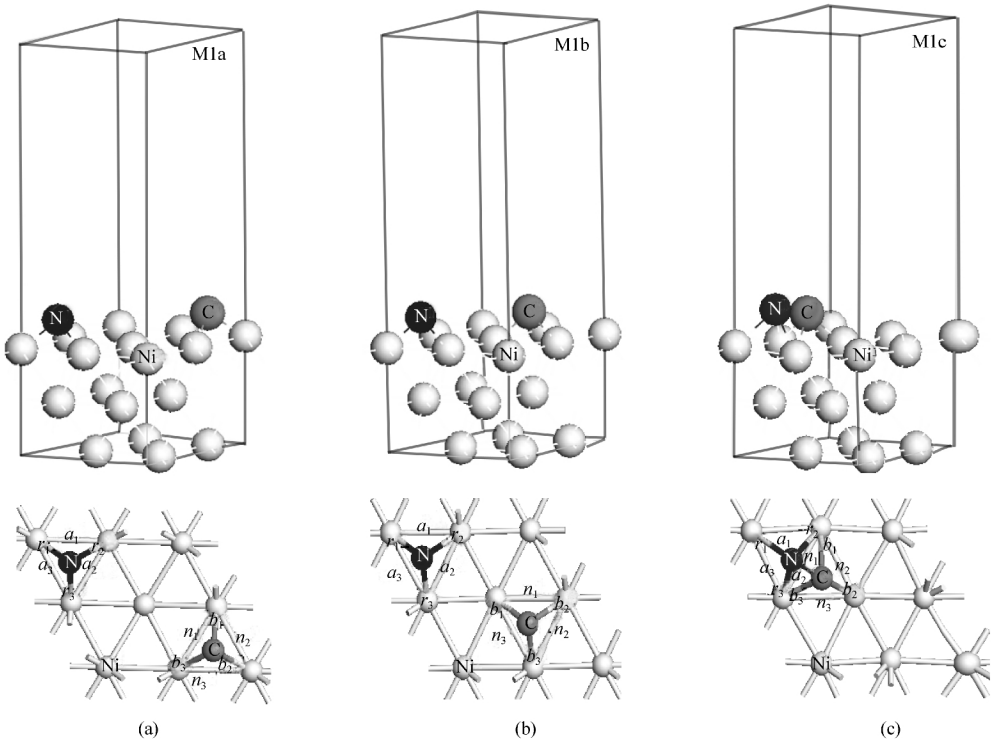

Fig.1 Side and top views of the Ni(111)-*p*(2×2)-(C+N) coadsorption systems at a coverage of 0.25 ML with the nitrogen atom adsorbed at the hcp hollow site

(a) and (b) are the Ni(111)-*p*(2×2)-(C+N) coadsorption systems with the carbon atoms adsorbed at the fcc and hcp hollow sites on the opposite (1×1) unit cell with nitrogen respectively, while (c) means the carbon atom occupying the fcc hollow site on the same (1×1) unit cell with nitrogen. The white, grey, and black spheres represent Ni, C, and N atoms respectively.

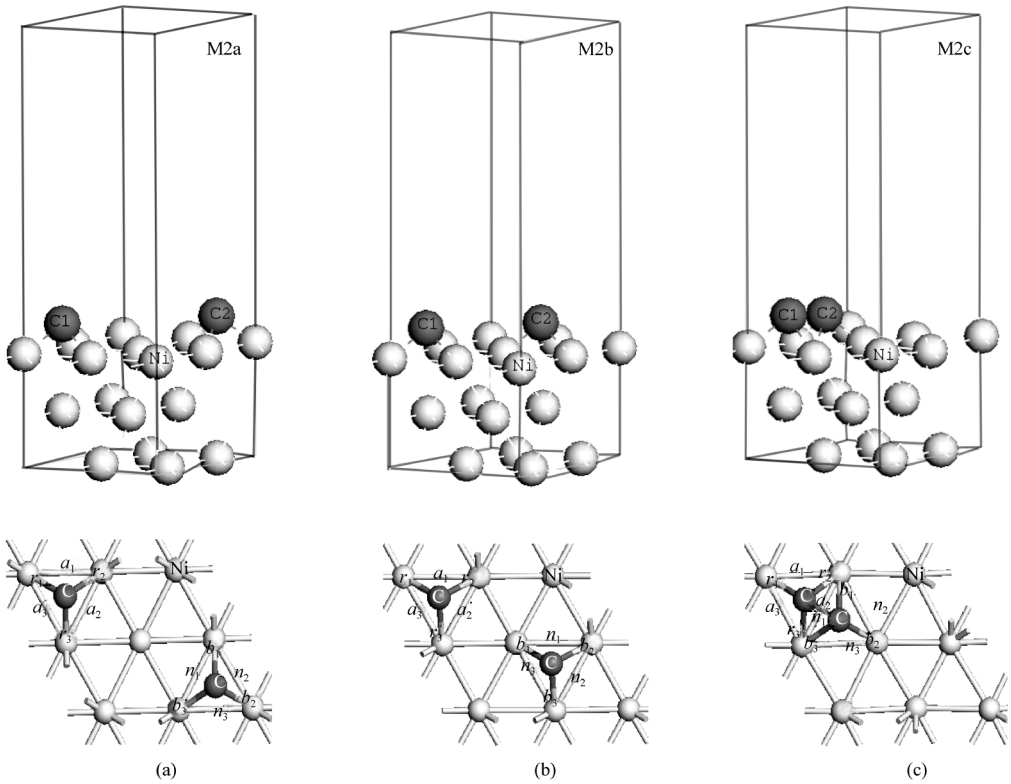

Fig.2 Side and top views of the Ni(111)-*p*(2×2)-C adsorption systems at a coverage of 0.5 ML

The white and grey spheres represent nickel and carbon atoms, respectively.

about 0.04 eV between the N atoms adsorbed at the hcp and fcc hollow sites on the Ni(111)-(2×2) surface at a coverage of 0.25 ML, three nonequivalent coadsorption systems could be built with the nitrogen atom adsorbed at the hcp hollow site and carbon atom varying its adsorption hollow sites successively as shown in Fig.1. These three models are represented by M1a, M1b, and M1c, respectively. For comparison, three Ni(111)-*p*(2×2)-C adsorption systems at a coverage of 0.5 ML, namely, the nitrogen atom in Fig.1 is replaced by a carbon atom, were built in Fig.2. For the two carbon adatoms, the one marked with 'C1' is the substitute for nitrogen, and the other one marked with 'C2' is the counterpoint of carbon in Fig.1. Accordingly, these three models are represented by M2a, M2b, and M2c, respectively. The Ni(111)-*p*(2×2)-N and Ni(111)-*p*(2×2)-C models at 0.25 ML were built and computed for comparison. The optimized bond lengths of N—Ni, C—Ni and bond angles of Ni—N—Ni and Ni—C—Ni in these models are shown in Table 1.

During the geometry optimization of all the models, the surface unit cells constrained all the parameters of the bottom two layers of Ni atoms, while the adsorbates and the topmost layer of the substrate were completely relaxed, and the lattice parameters were not optimized as well. According to our convergence test, in all of the calculations, the *k*-space was divided with the Monkhorst-Pack *k*-point grid of 6×6×1 within the Brillouin zones

Table 1 Calculated values of coadsorption energies and total adsorption energies, interaction energies and the optimized distances between the adatoms, the optimized bond lengths of N—Ni, C—Ni and bond angles of Ni—N—Ni, Ni—C—Ni

Adsorption system	E_{coads} or E_{totads}/eV	E_{int}/eV	D_{N-C} or D_{C-C}/nm	Bond length (nm)	Bond angle (°)
M1a	−12.389	1.372	0.2876	$r_1=r_2=r_3=0.1784$, $b_1=b_3=0.1764$, $b_2=0.1765$	$a_1=87.419$, $a_2=87.378$, $a_3=87.420$, $n_1=91.120$, $n_2=91.056$, $n_3=91.060$
M1b	−12.193	1.615	0.2492	$r_1=0.1755$, $r_2=r_3=0.1800$, $b_1=0.1740$, $b_2=0.1802$, $b_3=0.1801$	$a_1=89.217$, $a_2=86.382$, $a_3=89.217$, $n_1=91.495$, $n_2=88.117$, $n_3=91.495$
M1c	−13.899	−0.138	0.1255	$r_1=0.2060$, $r_2=0.2082$, $r_3=0.2078$, $b_1=0.2009$, $b_2=0.1857$, $b_3=0.2005$	$a_1=73.112$, $a_2=78.760$, $a_3=73.195$, $n_1=73.112$, $n_2=78.760$, $n_3=73.195$
M2a	−13.137	1.560	0.2875	$r_1=0.1779$, $r_2=r_3=0.1780$, $b_1=0.1776$, $b_2=0.1774$, $b_3=0.1775$	$a_1=88.845$, $a_2=88.785$, $a_3=88.840$, $n_1=89.213$, $n_2=89.203$, $n_3=89.215$
M2b	−13.125	1.619	0.2491	$r_1=0.1741$, $r_2=r_3=0.1812$, $b_1=0.1739$, $b_2=b_3=0.1813$	$a_1=90.760$, $a_2=86.988$, $a_3=90.770$, $n_1=90.924$, $n_2=86.725$, $n_3=90.917$
M2c	−14.921	−0.224	0.1330	$r_1=0.1851$, $r_2=0.1966$, $r_3=0.1965$, $b_1=0.1983$, $b_2=0.1841$, $b_3=0.1982$	$a_1=81.565$, $a_2=83.646$, $a_3=81.624$, $n_1=82.792$, $n_2=82.622$, $n_3=82.746$

of the $p(2\times2)$ supercell, and the plane-wave energy cutoff used was 330.0 eV. And the scheme used for geometry optimization was Broyden Fletcher Goldfarb Shanno (BFGS)[24]. Spin polarization was included in all the calculations. The convergence threshold for the total energy, maximum force, and maximum displacement were 0.001 eV, 0.3 eV·nm^{-1}, and 0.0002 nm, respectively.

2 Results and discussion

2.1 Adsorption and interaction energy analysis

Firstly, the adsorption energies of per adatom on a Ni(111)-(2×2) surface at a coverage of 0.25 ML were calculated, and it is defined as shown in Eq.(1),

$$E_{ads}=E_{Ni:A}-E_{Ni}-E_A \quad (1)$$

where, $E_{Ni:A}$ (A=C, N) is the total energies of the adsorption systems, E_{Ni} is the energy of the Ni(111)-(2×2) clean surface, and E_A(A=C, N) represents the spin polarized energy of a free adatom, which is −147.637 and -266.022 eV for C and N atoms, respectively. For the models in Fig.1 and Fig.2, the coadsorption energy of nitrogen and carbon atoms and the total adsorption energy of carbon atoms were calculated with Eqs.(2) and (3), respectively[25],

$$E_{coads}=E_{Ni:(C+N)}-E_{Ni}-E_C-E_N \quad (2)$$

$$E_{totads}=E_{Ni:2C}-E_{Ni}-2E_C \quad (3)$$

where, $E_{Ni:(C+N)}$ is the total energy of the Ni(111)-p(2×2)-(C+N) system, and $E_{Ni:2C}$ is the total energy of the Ni(111)-p(2×2)-C system at a coverage of 0.5 ML. Furthermore, for the models in Fig. 1 and Fig.2, the interaction energies between the adatoms were calculated with Eqs.(4) and (5), respectively[26], as follows:

$$E_{int}=E_{coads}-E_{ads:N}-E'_{ads:C} \quad (4)$$

$$E_{int}=E_{totads}-E_{ads:C}-E'_{ads:C} \quad (5)$$

where, $E_{ads:N}$ and $E_{ads:C}$ represent the adsorption energies of nitrogen and carbon atoms in the Ni(111)-p(2×2)-N and Ni(111)-p(2×2)-C system at a coverage of 0.25 ML with the adatom locating at the hcp hollow sites, while $E'_{ads:C}$ is the adsorption energy of carbon atom in the Ni(111)-p(2×2)-C system at a coverage of 0.25 ML, but with the carbon atom occupying different hollow sites according to the models in Fig.1 and Fig.2, namely, fcc for M1a, M2a, M1c, and M2c, and hcp for M1b and M2b. The calculated values of coadsorption energies of nitrogen and carbon atoms (E_{coads}), total adsorption energies of double carbon atoms (E_{totads}), the interaction energies between the adatoms (E_{int}) along with the optimized distance (D) between the adatoms are summarized in Table 1. For the optimized distance between the adatoms, the translational invariance was considered.

As shown in Table 1, when they are in the same (1×1) unit cell as shown in M2c, the two carbon adatoms have a distance of 0.1330 nm that is comparable with the C—C bond length of 0.142 nm in graphite[27], which may imply the formation of graphite state. Moreover, when the nitrogen atom in Fig.1 is replaced by a carbon atom as shown in Fig.2, the corresponding total adsorption energy of double carbon atoms is more negative than the coadsorption energy of nitrogen and carbon atoms, which suggests a more stable structure, and the C−C interaction energy also increases after this substitution. The positive interaction energies in M1a, M1b, M2a, and M2b show the common repulsion effect in the coadsorption and adsorption models, while the negative interaction energies in M1c and M2c suggest the adatoms bond. In addition, as the repulsion energies are high enough comparing with the coadorption energies and total adsorption energies in M1a, M1b, M2a, and M2b, the interaction between the adatoms can not be omitted.

2.2 Electronic structure analysis

The DOS plots provide another insight into the influence of atomic nitrogen on carbon on the Ni(111)-(2×2) surface. For carbon adsorbed at the fcc and hcp hollow sites on the Ni(111) surface with a coverage of 0.25 ML, the computed PDOSs are shown in Fig.3, which agree well with Klinke′s results[26]. The Fermi levels for these two Ni(111)-p(2×2)-C systems at 0.25 ML are −2.822 eV (fcc) and −2.795 eV (hcp), respectively, and it also can be seen that the carbon atoms almost have the same DOS whatever hollow site (fcc, hcp) it is adsorbed at.

In contrast, the PDOSs of the coadsorption and 0.5 ML carbon adsorption models in Fig.1 and Fig.2 are calculated. For the N and C atoms in the systems, the PDOSs are shown in Fig.4. For M1a, M1b, and M1c, the Fermi levels are −2.693, −2.695, and −2.518 eV, respectively. So the differences are rather small. M2a, M2b, and M2c, have the similar Fermi levels of −2.592, −2.578, and −2.619 eV, too. In comparison with Fig.3, the carbon-nickel bonding bands approximately 11 eV below the Fermi level become broader for models of M2a and M2b. The direct

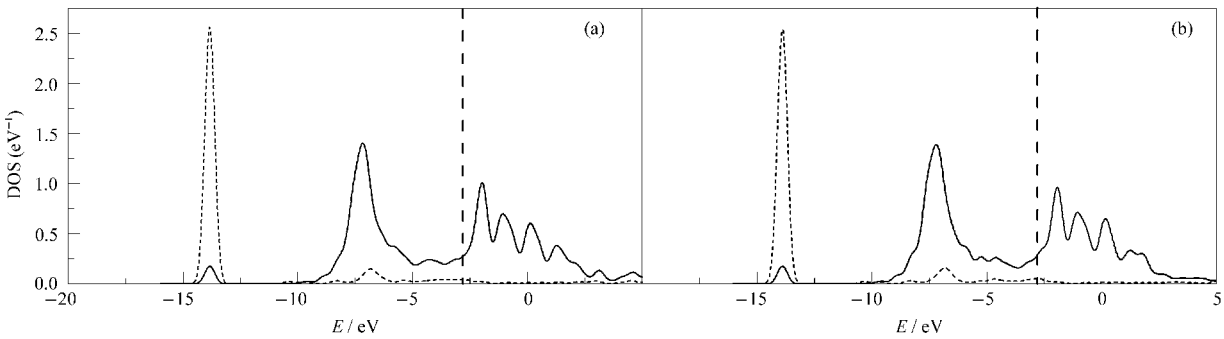

Fig.3 PDOSs of carbon atom in the Ni(111)-p(2×2)-C system at 0.25 ML with the carbon atom adsorbed at the fcc hollow site (a) and hcp hollow site (b)

The C(2s) and C(2p) orbital contributions are represented by dashed line and solid line, respectively. The vertical dashed line denotes the Fermi level.

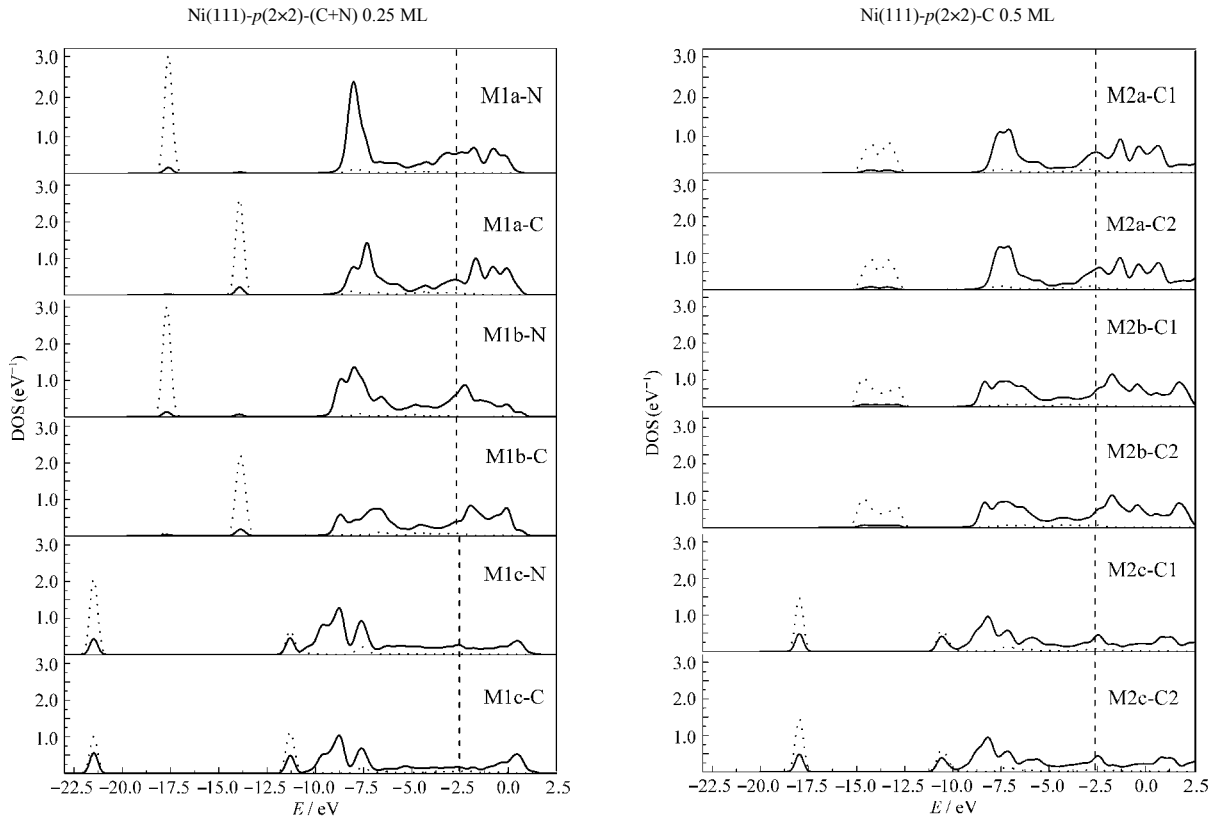

Fig.4 PDOSs of the N and C atoms in the adsorption systems

The M1a-N, M1a-C, M1b-N, M1b-C, M1c-N, and M1c-C plots correspond to the N and C atoms in the models of M1a, M1b, and M1c, while M2a-C1, M2a-C2, M2b-C1, M2b-C2, M2c-C1, and M2c-C2 plots correspond to the 'C1' and 'C2' atoms in the models of M2a, M2b, and M2c, respectively. The 2*s* and 2*p* orbital contributions are represented by dotted line and solid line, respectively. The vertical dashed line denotes the Fermi level.

C–C interactions rather than indirect interactions through the nickel surface result in this breadth. On the other hand, the almost unchanged shape of this band for models of M1a and M1b reveals a weaker C–N interaction compared with the C–C interaction. In addition, for the models of M1b and M2b, another change is observed for the formation of N—C and C—C bonding band at about −8.0 eV. Furthermore, as the nitrogen and carbon or the double carbon atoms are in the same (1×1) unit cell, the corresponding PDOSs shown in M1c-C and M2c-C2(Fig.4) indicate great change. The N—C or C—C bonding states at about −21.0 and −18.0 eV become evident.

However, the most striking character of these PDOSs is the number of orbitals at their Fermi levels, which is an important criterion for the extent of a carbon atom catalyzed by nickel catalyst. Hence, for the carbon atoms adsorbed on the two Ni(111)-*p*(2×2)-C systems at 0.25 ML and the carbon atoms which vary their adsorption hollow sites in the models of Fig.1 and Fig.2, the DOSs of C(2*s*+2*p*) at the Fermi level are summarized in Table 2 with spline fitting. As can be seen, carbon atoms are not easy to be catalyzed at lower coverage on catalyst surface. Even the nitrogen atoms can improve the catalysis to some extent, but the effect is not evident in comparison with the C–C interactions. This can be used to explain the existence of different types of nitrogen-contained diamonds and the inhibition of atomic nitrogen on carbon conversion in diamond synthesis. However, if the nitrogen and carbon or the carbon atoms were much too close as shown in M1c and M2c, the CN compounds or graphite-like impurities may appear. Therefore, the nitrogen atoms not only occupy some nickel catalysis surface, but also inhibit the catalyst effect in the diamond synthesis.

Table 2 The DOS of C(2*s*+2*p*) at the Fermi levels

Adsorption system	DOSs at Fermi level (eV^{-1})	Adsorption system	DOSs at Fermi level (eV^{-1})
Ni(111)-*p*(2×2)-C (0.25 ML fcc)	0.320	Ni(111)-*p*(2×2)-C (0.25 ML hcp)	0.343
M1a	0.470	M2a	0.643
M1b	0.469	M2b	0.528
M1c	0.228	M2c	0.466

3 Conclusions

Coadsorption models were built to study the catalytic action of nickel in diamond synthesis. The substrate and adatoms served as the catalyst and reactants, respectively. For the adatom, the number of orbitals at their Fermi level was used to estimate the effect of catalyst. The models built in this work conveniently simulated the coexistence of carbon and nitrogen atoms in the diamond synthesis. Our theoretical values explained the experimental phenomenon effectively that the atom-

ic nitrogen inhibits the carbon conversion in diamond synthesis. According to the comparison of the Ni(111)-p(2×2)-(C+N) coadsorption system at 0.25 ML with the Ni(111)-p(2×2)-C adsorption system at 0.5 ML on adsorption energy, interaction energy and PDOS at the Fermi level, we concluded that the appearance of nitrogen atoms made the adsorption system relatively unstable, and the interaction between the adatoms in both systems can not be omitted. According to the interaction energies, the C–C interaction was stronger than the C–N interaction. In addition, the PDOS differences among these models, which were induced mainly by the interaction between the adatoms, suggested that the existence of nitrogen atoms could also improve the catalysis to some extent, but the effect was not evident in comparison with the C–C interaction. This could be used to explain the existence of different types of nitrogen-contained diamonds and the inhibition of atomic nitrogen on carbon conversion in diamond synthesis. However, the obtained atomic geometry and PDOS also indicated the formation of CN compounds or graphite-like impurities if the adatoms distance was much too short as they occupied the same (1×1) unit cell. The models and approach used in this article can be helpful for finding new kinds of catalysts in diamond synthesis.

References

1 Larico, R.; Justo, J. F.; Machado, W. V. M.; Assali, L. V. C. *Physica B*, **2003, 340–342**: 84

2 Tong, X. L.; Zhao, G. H.; Xiao, X. E.; Hu, H. K. *Acta Phys. -Chim. Sin.*, **2008, 24**(3): 416 [童希立, 赵国华, 肖小娥, 胡惠康. 物理化学学报, **2008, 24**(3): 416]

3 Blank, V.; Popov, M.; Pivovarov, G.; Lvova, N.; Terentev, S. *Diam. Relat. Mat.*, **1999, 8**: 1531

4 Kaiser, W.; Bond, W. L. *Phys. Rev.*, **1959, 115**: 857

5 Slack, G. A. *J. Appl. Phys.*, **1964, 35**: 3460

6 Liang, Z. Z.; Kanda, H.; Jia, X.; Ma, H. A.; Zhu, P. W.; Guan, Q. F.; Zang, C. Y. *Carbon*, **2006, 44**: 913

7 Borzdov, Y.; Pal′yanov, Y.; Kupriyanov, I.; Gusev, V.; Khokhryakov, A.; Sokol, A.; Efremov, A. *Diam. Relat. Mat.*, **2002, 11**: 1863

8 Kanda, H.; Akaishi, M.; Yamaoka, S. *Diam. Relat. Mat.*, **1999, 8**: 1441

9 Lombardi, E. B.; Mainwood, A.; Osuch, K.; Reynhardt, E. C. *J. Phys. -Condens. Matter*, **2003, 15**: 3135

10 Liu, Y. Y.; Bauer-Grosse, E.; Zhang, Q. Y. *Acta Phys. Sin.*, **2007, 56**(4): 2359 [刘燕燕, Bauer-Grosse, E., 张庆愈. 物理学报, **2007, 56**(4): 2359]

11 Tang, C. J.; Neves, A. J.; Fernandes, A. J. S.; Grácio, J.; Carmo, M. C. *J. Phys. -Condens. Matter*, **2007**, **19**: 386236

12 Li, X. L.; Liu, W. M.; Xue, Z. Q.; Li, J. C.; Hou, S. M.; Zhang, Z. L.; Peng, L. M.; Shi, Z. J.; Gu, Z. N. *Acta Phys. -Chim. Sin.*, **2000, 16**(9): 772 [李秀兰, 刘惟敏, 薛增泉, 李建昌, 侯士敏, 张灶利, 彭练矛, 施祖进, 顾镇南. 物理化学学报, **2000, 16**(9): 772]

13 Sun, J.; Hu, S. L.; Du, X. W.; Lei, Y. W.; Jiang, L. *Acta Phys. -Chim. Sin.*, **2007, 23**(7): 1105 [孙 景, 胡胜亮, 杜希文, 雷贻文, 江 雷. 物理化学学报, **2007, 23**(7): 1105]

14 Liang, Z. Z.; Jia, X.; Zang, C. Y.; Zhu, P. W.; Ma, H. A.; Ren, G. Z. *Diam. Relat. Mat.*, **2005, 14**: 243

15 Liu, Y. L.; Kong, F. J.; Yang, B. W.; Jiang, G. *Acta Phys. Sin.*, **2007, 56**(9): 5413 [刘以良, 孔凡杰, 杨缤维, 蒋 刚. 物理学报, **2007, 56**(9): 5413]

16 Segall, M. D.; Lindan, P. J. D.; Probert, M. J.; Pickard, C. J.; Hasnip, P. J.; Clark, S. J.; Paynel, M. C. *J. Phys. -Condens. Matter*, **2002, 14**: 2717

17 Vanderbilt, D. *Phys. Rev. B*, **1990, 41**: 7892

18 Perdew, J. P.; Chevary, J. A.; Vosko, S. H.; Jackson, K. A.; Pederson, M. R.; Singh, D. J.; Fiolhais, C. *Phys. Rev. B*, **1992, 46**: 6671

19 Hammer, B.; Hansen, L. B.; Norskov, J. K. *Phys. Rev. B*, **1999, 59**: 7413

20 Perdew, J. P.; Burke, K.; Ernzerhof, M. *Phys. Rev. Lett.*, **1996, 77**: 3865

21 Shelton, J. C.; Patil, H. R.; Blakely, J. M. *Surf. Sci.*, **1974, 43**: 493

22 Villars, P. Pearson′s handbook: crystallographic data for intermetallic phases. Materials Park, OH: ASM International, 1997

23 Taylor, A. J. *Inst. Metals.*, **1950, 77**: 585

24 Pfrommer, B. G.; Cote, M.; Louie, S. G.; Cohen, M. L. *J. Comput. Phys.*, **1997, 131**: 233

25 Zhao, X. X.; Tao, X. M.; Chen, W. B.; Chen, X.; Shang, X. F.; Tan, M. Q. *Acta Phys. Sin.*, **2006, 55**(7): 3629 [赵新新, 陶向明, 陈文彬, 陈 鑫, 尚学府, 谭明秋. 物理学报, **2006, 55**(7): 3629]

26 Klinke, D. J. II; Wilke, S.; Broadbelt, L. J. *J. Catal.*, **1998, 178**: 540

27 Nixon, D. E.; Parry, G. S. *J. Phys. C*: *Solid State Phys.*, **1969, 2**: 1732